Supporting Information

Experimental Section

Synthesis of a-MnO_2

All reagents were analytical reagent grade without further purification. Typically, $KMnO_4$ (50 mg) and $NaH_2PO_2 \cdot H_2O$ (70 mg) were respectively dissolved in 60 mL deionized water to generate $KMnO_4$ solution and NaH_2PO_2 solution. Then, $KMnO_4$ solution was quickly added to NaH_2PO_2 solution at 35°C with constant stirring. Afterwards, the mixed solution was cooled down to room temperature and the precipitates were collected by centrifuging, washed twice with deionized water, and finally dried at 60 °C for 12 h to obtain a-MnO_2. c-MnO_2 was prepared by annealing a-MnO_2 in O_2 atmosphere for 2 h.

Electrochemical experiments in MEA cell

Electrochemical experiments were conducted using a zero-gap membrane electrode assembly (MEA) electrolyzer. The setup consisted of two titanium current collector plates (cathode and anode) with serpentine flow channels, separated by two 300 μm PTFE gaskets. All potentials were referenced to a reversible hydrogen electrode (RHE) by E (V vs. RHE) = E (V vs. Ag/AgCl) + 0.198 V + 0.059 × pH. The catalyst slurry was prepared by dissolving 25 mg of the catalyst in 3 mL of isopropanol with 20 μL of Nafion ionomer solution (5 wt% in H_2O). Next, the catalyst slurry was slowly dropped onto the carbon paper (Sigracet 29 BC) to attain a catalyst loading of ~0.5 mg cm^{-2} as a gas diffusion layer (GDL). Nickel mesh was used as the anode and Ag/AgCl served as the reference electrode. An anion exchange membrane (Fumasep FAA-3-PK-75) was used to separate the cathode and anode chambers. The catholyte was a solution containing 0.1 M $KHCO_3$, while the anolyte consisted of a 1 M KOH solution. The catholyte was purged with Ar prior to the electrochemical experiments. During the electrolysis, the humidified NO/CO_2 mixed gas was fed from the non-catalyst side of the GDL, while anolyte was continuously cycled at a rate of 20 mL min^{-1} under pump drive. After electrolysis for 1 h, the produced urea was quantitatively determined by the urease decomposition method.

Determination of urea

Urea concentration was detected via urease decomposition method[1]. Typically, 0.2 mL of urease solution with concentration of 5 mg mL^{-1} was added into 2 mL of urea electrolyte, and the reaction is carried out in a thermostatic oscillator at 37°C for 40 min. Urea was decomposed by urease into CO_2 and two NH_3 molecules. After the decomposition, NH_3 concentration of urea electrolyte with urease (c_{urease}) was measured using the indole blue method. Meanwhile, NH_3 concentration contained in urea electrolyte without urease (c_{NH3}) was also quantified by indophenol blue method. The concentration of urea in the electrolyte (c_{urea}) was calculated by the following equation.

$$c_{urea} = (c_{urease} - c_{NH3}) / 2 \quad (1)$$

The urea yield rate and FE_{urea} were calculated by the following equation:

$$\text{Urea yield rate} = (c_{urea} \times V) / (60.06 \times t \times A) \quad (2)$$

$$FE_{urea}\ (\%) = (10 \times F \times c \times V) / (60.06 \times Q) \times 100\% \quad (3)$$

where c_{urea} (μg mL^{-1}) is the measured urea concentration, V (mL) is the volume of the electrolyte, t (h) is the reduction time, A (cm^{-2}) is the surface area of cathode, F (96 500 C mol^{-1}) is the Faraday constant, Q (C) is the quantity of applied electricity.

Determination of NH_3

NH_3 in electrolyte was quantitatively determined by the indophenol blue method[2]. Typically, 2 mL of electrolyte was removed from the electrochemical reaction vessel and diluted with deionized water. Then 2 mL of diluted solution was removed into a clean vessel followed by sequentially adding NaOH solution (2 mL, 1 M) containing $C_7H_6O_3$ (5 wt.%) and $C_6H_5Na_3O_7$ (5 wt.%), NaClO (1 mL, 0.05 M), and $C_5FeN_6Na_2O$ (0.2 mL, 1wt.%) aqueous solution. After the incubation for 2 h at room temperature, the mixed solution was subjected to UV-vis measurement using the absorbance at 655 nm wavelength. The concentration-absorbance curves were calibrated by the standard NH_4Cl solution with a series of concentrations.

Characterizations

X-ray diffraction (XRD) was conducted on a Rigaku D/max 2400 diffractometer. Transmission electron microscopy (TEM) and high-resolution transmission electron microscopy (HRTEM) were performed on a Tecnai G2 F20 microscope at an

acceleration voltage of 200 kV. Electron paramagnetic resonance (EPR) measurements were conducted on a Bruker ESP-300 spectrometer. Online differential electrochemical mass spectrometry (DEMS, QAS 100) was carried out by QAS 100 spectrometer.

Calculation details

Density functional theory (DFT) calculations were carried out using a Cambridge sequential total energy package (CASTEP). The exchange-correlation function was utilized by Perdew-Burke-Ernzerhof (PBE) generalized gradient approximation (GGA) functional. To ensure all atoms were fully relaxed for each system, a cutoff energy of 400 eV was chosen and the 3 × 3 × 1 Monkhorst-Pack mesh was used in Brillouin zone sampling. The model was optimized to converge the absolute energy to 1.0×10^{-5} eV with a force convergence of 0.02 eV $Å^{-1}$. The Gibbs free energy (ΔG, 298 K) of reaction steps is calculated by:

$$\Delta G = \Delta E + \Delta ZPE - T\Delta S \quad (4)$$

where ΔE is the adsorption energy, ΔZPE is the zero-point energy difference and $T\Delta S$ is the entropy difference between the gas phase and adsorbed state. The entropies of free gases were acquired from the NIST database.

The adsorption energy (ΔE) is defined as:

$$\Delta E = E_{ads/slab} - E_{ads} - E_{slab} \quad (5)$$

where $E_{ads/slab}$, E_{ads} and E_{slab} are the total energies for adsorbed species on slab, adsorbed species and isolated slab, respectively. The transition states of each reaction steps are analyzed by a combined linear synchronous transit and quadratic synchronous transit tools (LST/QST)[3].

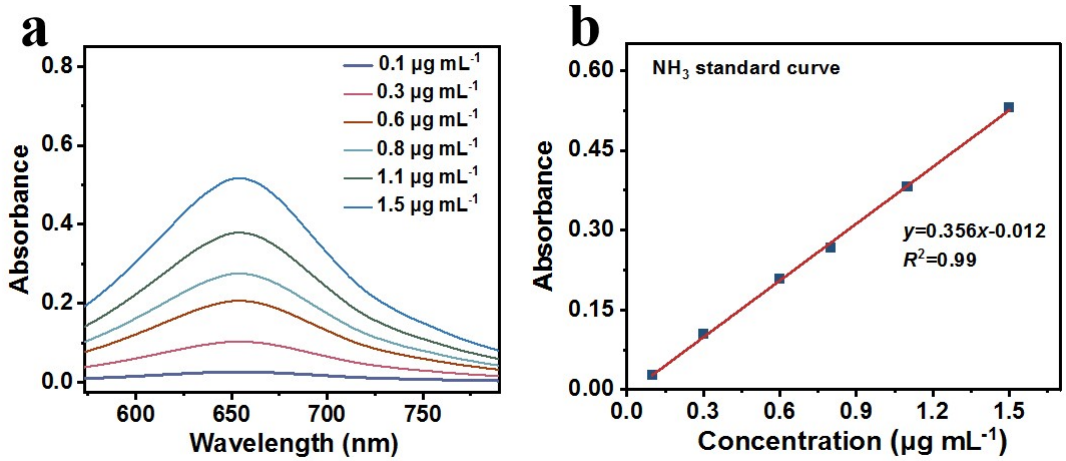

Fig. S1. (a) UV-vis absorption spectra of NH_4Cl assays after incubated for 2 h at ambient conditions. (b) Calibration curve used for the calculation of NH_3 concentrations.

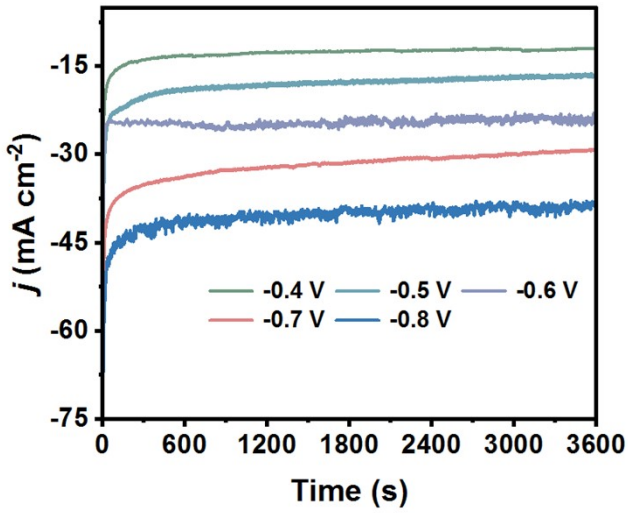

Fig. S2. Chronoamperometry curves of a-MnO_2 at various potentials after 1 h of EUCN electrolysis.

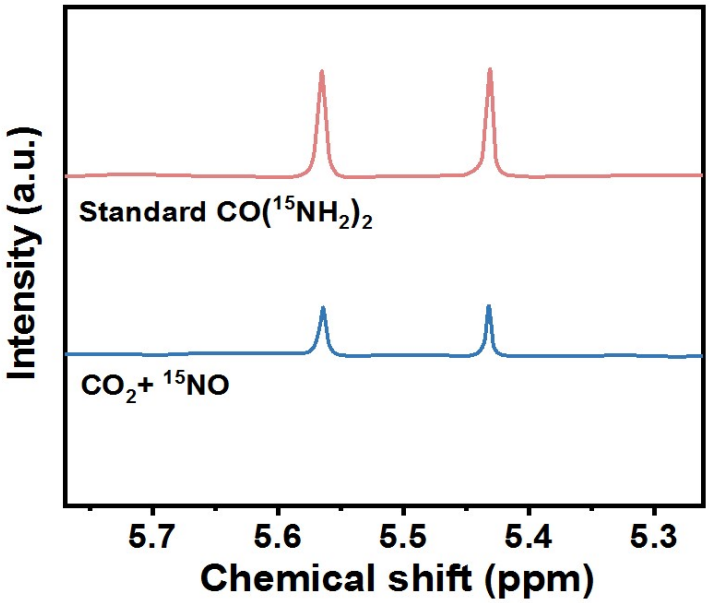

Fig. S3. ^{1}H NMR spectra of $CO(^{15}NH_2)_2$ standard sample and those fed by ^{15}NO after electrolysis at -0.7 V.

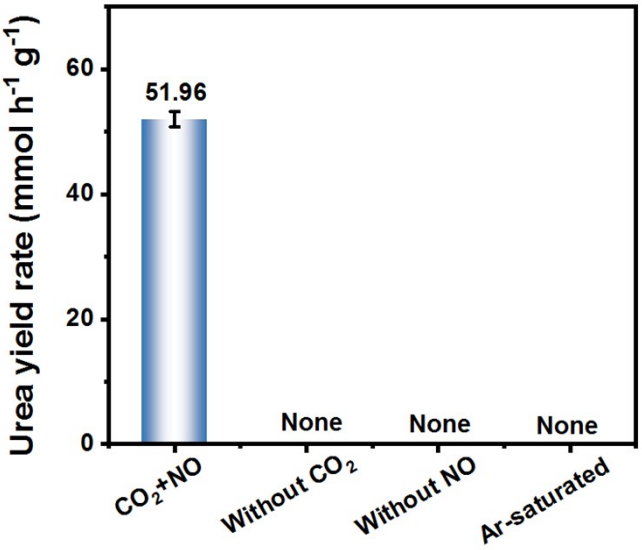

Fig. S4. Amounts of produced urea on a-MnO_2 under different conditions: (1) electrolysis in a mixed CO_2/NO-saturated gas electrolyte at -0.7 V, (2) electrolysis in NO-saturated but CO-free electrolyte at -0.7 V, (3) electrolysis in CO_2-saturated but NO-free electrolyte at -0.7 V, (4) electrolysis in Ar-saturated electrolyte at -0.7 V.

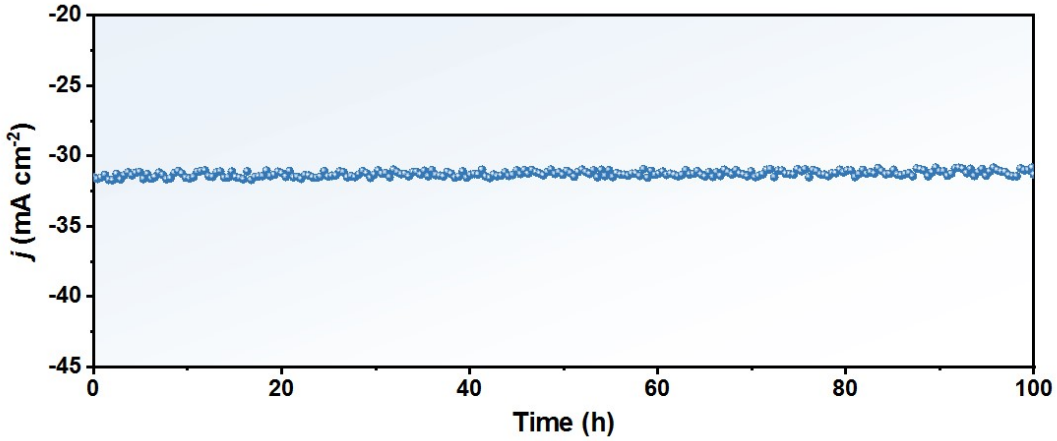

Fig. S5. Long-term stability test of a-MnO_2 in MEA at -0.7 V.

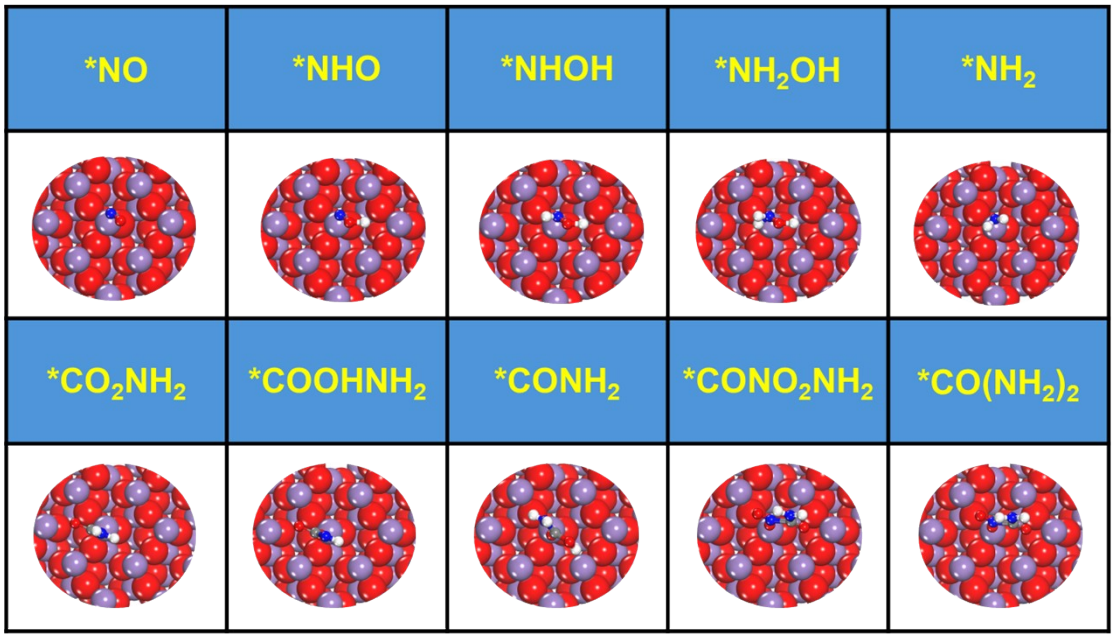

Fig. S6. Optimized atomic configurations of the reaction intermediates on c-MnO_2.

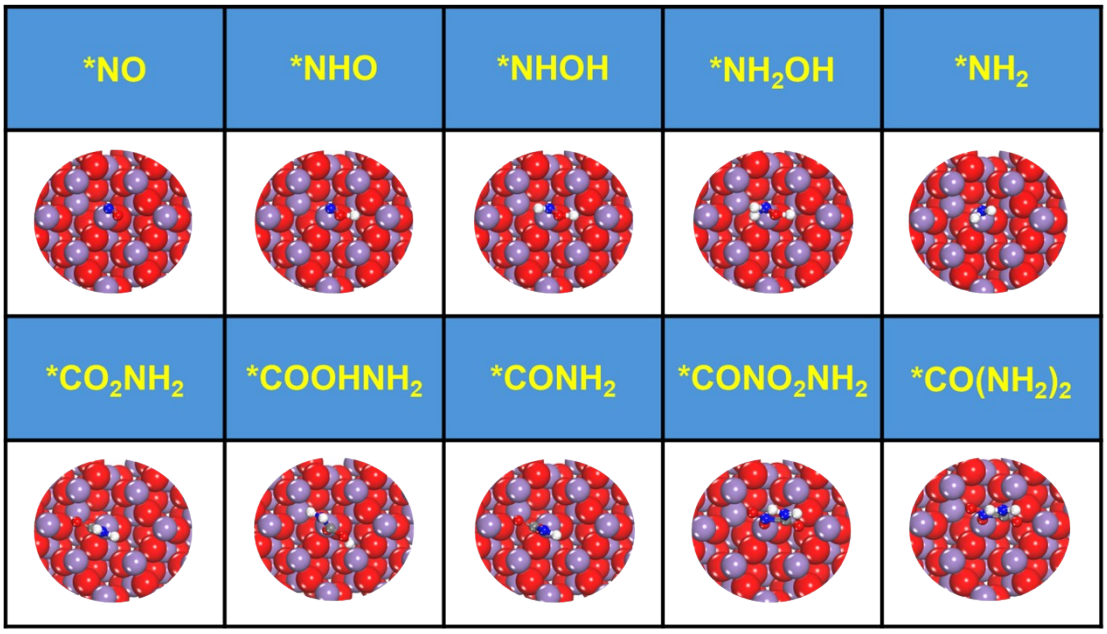

Fig. S7. Optimized atomic configurations of the reaction intermediates on a-MnO_2.

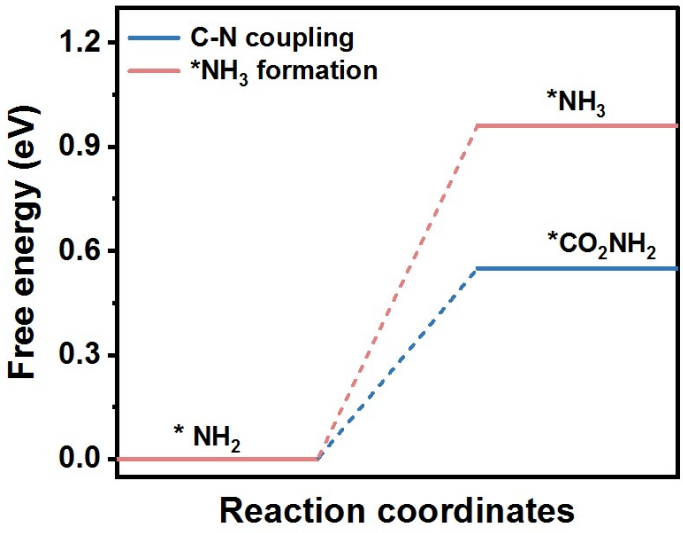

Fig. S8. Free energy profiles of competition between $*NH_2 \rightarrow *CO_2NH_2$ and $*NH_2 \rightarrow *NH_3$ conversion on a-MnO_2.

Table S1. Comparison of the optimum urea yield rate and FE_{urea} for the recently reported state-of-the-art urea electrocatalysts at ambient conditions.

Catalyst	**C/N sources**	**Urea yield rate (mmol g^{-1} h^{-1})**	**FE_{urea} (%)**	**Potential (V vs. RHE)**	**Ref.**
InOOH	CO_2 +N_2	6.85	20.97	-0.4	4
Pd_1Cu_1-TiO_2	CO_2 +N_2	10.0	22.54	-0.5	5
Zn-Mn	CO_2 +N_2	4.14	63.5	-0.3	6
$CoRuN_6$	CO_2 +NO_3^-	8.98	25.31	-0.6	7
Cu-Bi	CO_2 +NO_3^-	36.3	23.5	-0.6	8
VB_{12}-CNTs	CO_2 +NO_3^-	2.73	26.04	-0.5	9
Co-O-C	CO_2 +NO_3^-	45.03	31.4	-1.5	10
$SrRuO_3$	CO_2 +NO_3^-	25.07	34.1	-0.7	11
Cu-Ni	CO_2 +NO_3^-	22.01	25.1	-0.5	12
Zn NBs	CO_2 +NO	15.13	11.16	-0.92	13
a-MnO_2	**CO_2 +NO**	**51.96**	**36.69**	**-0.7**	**This work**

References

1. X. Wei, X. Wen, Y. Liu, C. Chen, C. Xie, D. Wang, M. Qiu, N. He, P. Zhou and W. Chen, *J. Am. Chem. Soc.*, 2022, **144**, 11530-11535.
2. P. Li, Z. Jin, Z. Fang and G. Yu, *Energy Environ. Sci.*, 2021, **14**, 3522-3531.
3. Q. Jiang, Z. Ao and Q. Jiang, *Phys. Chem. Chem. Phys.*, 2013, **15**, 10859-10865.
4. M. Yuan, J. Chen, Y. Xu, R. Liu, T. Zhao, J. Zhang, Z. Ren, Z. Liu, C. Streb and H. He, *Energy Environ. Sci.*, 2021, **14**, 6605-6615.
5. L. Pan, J. Wang, F. Lu, Q. Liu, Y. Gao, Y. Wang, J. Jiang, C. Sun, J. Wang and X. Wang, *Angew. Chem.*, 2023, **135**, e202216835.
6. X. Zhang, X. Zhu, S. Bo, C. Chen, K. Cheng, J. Zheng, S. Li, X. Tu, W. Chen and C. Xie, *Angew. Chem.*, 2023, **135**, e202305447.
7. C. Liu, H. Tong, P. Wang, R. Huang, P. Huang, G. Zhou and L. Liu, *Appl. Catal., B*, 2023, **336**, 122917.
8. X. Song, X. Ma, T. Chen, L. Xu, J. Feng, L. Wu, S. Jia, L. Zhang, X. Tan and R. Wang, *J. Am. Chem. Soc.*, 2024, **146**, 25813-25823.
9. M. Cong, Q. Liu, D. Wang, S. Hao, Z. Han, H. Xu, M. Guo, X. Ding and Y. Gao, *Appl. Catal., B*, 2024, **351**, 123941.
10. S. Zhang, M. Jin, H. Xu, X. Zhang, T. Shi, Y. Ye, Y. Lin, L. Zheng, G. Wang, Y. Zhang, H. Yin, H. Zhang and H. Zhao, *Energy Environ. Sci.*, 2024, **17**, 1950-1960.
11. L. Lv, H. Tan, Y. Kong, B. Tang, Q. Ji, Y. Liu, C. Wang, Z. Zhuang, H. Wang and M. Ge, *Angew. Chem.*, 2024, **136**, e202401943.
12. Y. Zhou, B. Yang, Z. Huang, G. Chen, J. Tang, M. Liu, X. Liu, R. Ma, Z. Mei and N. Zhang, *Appl. Catal., B*, 2024, **343**, 123577.
13. Y. Huang, R. Yang, C. Wang, N. Meng, Y. Shi, Y. Yu and B. Zhang, *ACS Energy Lett.*, 2021, **7**, 284-291.